

## Assessing Cloud-Phase Conditions

STEWART G. COBER, GEORGE A. ISAAC, ALEXEI V. KOROLEV, AND J. WALTER STRAPP

*Cloud Physics Research Division, Meteorological Service of Canada, Downsview, Ontario, Canada*

(Manuscript received 13 September 2000, in final form 23 April 2001)

### ABSTRACT

In situ microphysics measurements made during the First and Third Canadian Freezing Drizzle Experiments (CFDE I and III, respectively) have been used to assess the relative responses to ice and liquid hydrometeors for several common instruments. These included the Rosemount icing detector, 2D-C monoscale and 2D-C grayscale probes, forward-scattering spectrometer probes (FSSP) on three measurement ranges, Nevzorov liquid water content (LWC) and total water content probes, and King LWC probes. The Nevzorov LWC and King LWC probes responded to between 5% and 30% of the ice water content, with an average response of approximately 20%. The average FSSP measurements of droplet spectra were dominated by ice particles for sizes greater than  $35\ \mu\text{m}$ , independent of the measurement range used, when the ice-crystal concentrations exceeded approximately  $1\ \text{L}^{-1}$ . In contrast, the FSSP measurements of the droplet spectra less than  $30\ \mu\text{m}$  appeared free of ice-crystal contamination, independent of the ice-crystal concentrations observed. Glaciated cloud conditions always had FSSP-measured median volume diameters greater than  $30\ \mu\text{m}$  and particle concentrations less than  $15\ \text{cm}^{-3}$ , whereas similar measurements in entirely liquid-phase clouds were observed less than 4% of the time. Images of drops greater than or equal to  $125\ \mu\text{m}$  in diameter, which were collected in warm clouds greater than  $0^\circ\text{C}$ , were used to calibrate geometric criteria, which were, in turn, used to segregate 2D images into circular and noncircular categories. It is shown that, on average, between 5% and 40% of ice crystals greater than or equal to  $125\ \mu\text{m}$  in diameter will be classified as circular, depending on the particle size, with the percentage decreasing with increasing particle size. In liquid-phase clouds, between 85% and 95% of the 2D images will be correctly classified as circular for all particle sizes. At temperatures less than  $-4^\circ\text{C}$ , a Rosemount icing-detector threshold of  $2\ \text{mV s}^{-1}$ , corresponding to a maximum LWC of  $0.002\ \text{g m}^{-3}$ , was used to help to identify glaciated and nonglaciated conditions. A methodology for segregating liquid, mixed, and glaciated cloud regions, based on instrument responses to liquid and ice hydrometeors, was developed and applied to the CFDE dataset. The results were used to determine the relative frequency of liquid, mixed, and glaciated cloud conditions for the data collected during the two field projects. Approximately 40% of the in-cloud observations at temperatures less than  $0^\circ\text{C}$  were assessed as liquid phase. The fractions of mixed-phase and glaciated-phase conditions were 26% and 34% for CFDE I and 46% and 14% for CFDE III, respectively. Because the ice-crystal responses for each instrument depend on the aircraft sampling speed and the ice-crystal sizes and concentrations, the results may be limited to conditions similar to those in clouds in midlatitude winter storms. Regardless, the results may have application to several fields, including development of parameterizations for numerical modeling, precipitation formation, remote sensing, ice multiplication, radiative transfer, and aircraft icing investigations. Important implications for aircraft icing investigations are discussed.

### 1. Introduction

There are many applications that require accurate measurements of cloud liquid water content (LWC) and droplet spectra. For example, aircraft icing characterizations normally use the cloud LWC and droplet spectrum median volume diameter (Ashenden and Marwitz 1998; Cober et al. 1996; Miller et al. 1998). These measurements can become biased when ice crystals are present, because the majority of instruments designed for making in situ measurements respond to both liquid and ice hydrometeors. Cober et al. (1995) discussed how a

Particle Measuring Systems, Inc., (PMS) King probe measured an artificial LWC as high as  $0.1\ \text{g m}^{-3}$  in glaciated clouds, and Korolev et al. (1998b) estimated that the SkyTech Research, Inc., Nevzorov LWC probe could show an artificial LWC of 10% of the ice water content (IWC) in glaciated clouds. Strapp et al. (1999) have shown that the Nevzorov and King probes respond to as much as 40% of the IWC for faster-flying aircraft in certain meteorological situations. Gardiner and Hallett (1985) showed that PMS forward-scattering spectrometer probes (FSSP) responded significantly to ice crystals, and the misinterpretation of droplets as ice crystals with PMS 2D-C measurements has been discussed by Rauber and Heggli (1988). These biases might be considered to be insignificant if mixed-phase conditions represented a small fraction of the observed

---

*Corresponding author address:* Stewart Cober, Cloud Physics Research Division, Meteorological Service of Canada, Environment Canada, 4905 Dufferin Street, Downsview, ON M3H 5T4, Canada.  
E-mail: stewart.cober@ec.gc.ca

TABLE 1. Summary of instruments on the Convair-580 that are relevant to this investigation.

Instrument	Variable
Sensor Systems, Goodrich Corporation, Rosemount temperature sensor ( $\times 2$ )	Temperature
Reverse-flow temperature sensor	Temperature
Cambridge Systems, Inc. (now EdgeTech), dewpoint hygrometer	Dewpoint
Pitot tube ( $\times 3$ )	Air speed, pressure
Rosemount-858 probe	Air speed, pressure
PMS King LWC probe ( $\times 2$ )	Liquid water content
SkyTech Research, Inc., Nevzorov LWC probe	Liquid water content
SkyTech Research, Inc., Nevzorov TWC probe	Total water content
PMS FSSP 100 3–45 $\mu\text{m}$	Droplet concentration/size
PMS FSSP 100 5–95 $\mu\text{m}$	Droplet concentration/size
PMS 2D-C mono 25–800 $\mu\text{m}$	Hydrometeor concentration/size
PMS 2D-C gray 25–1600 $\mu\text{m}$	Hydrometeor concentration/size
PMS 2D-P mono 200–640 $\mu\text{m}$	Hydrometeor concentration/size
Sensor Systems, Goodrich Corporation, Rosemount icing detector	Icing accumulation rate

cloud conditions. However, this is not the case. In a review of mixed-phase observations, Riley (1998) found that mixed-phase conditions in clouds with temperatures less than  $0^{\circ}\text{C}$  were observed with a frequency of between 20% and 90%, depending on the region, environment, temperature, and instrumentation. These observations emphasize the requirement to be able to interpret and to segregate the ice- and liquid-based signals from instruments that are used for in situ measurements.

The importance of understanding the physics of mixed-phase conditions has been stressed in investigations for climate (Rotstajn 1997; Fowler and Randall 1996), radiative transfer (Sun and Shine 1994), numerical forecast modeling (Tremblay et al. 1996), microphysics, precipitation formation, and remote sensing (Young et al. 2000). Although these studies require accurate in situ measurements of both the liquid and ice hydrometeors, there are relatively few discussions about the capabilities and errors inherent with measurements made in mixed-phase environments. Although these characteristics are instrument and environment dependent, many research aircraft carry common suites of instruments, so a methodology for segregating ice and liquid hydrometeors may have a wide application. In this paper, the relative responses to ice and liquid particles will be discussed for several common instruments, and a methodology for segregating ice and liquid components will be presented. This methodology will be applied to a large dataset of observations collected in midlatitude winter storms.

## 2. Field projects

The data were obtained during the First and Third Canadian Freezing Drizzle Experiments (CFDE I and CFDE III, respectively). These projects are described in Isaac et al. (1998). The National Research Council Convair-580 aircraft was used as the instrument platform for both projects. CFDE I was conducted in March of 1995 and consisted of 12 flights over Newfoundland and the North Atlantic Ocean. CFDE III was conducted between December of 1997 and February of 1998 and

consisted of 26 flights over southern Ontario and Quebec, Lake Ontario, and Lake Erie. The primary objective for both projects was to obtain in situ microphysical data in winter storms for which supercooled large drops (SLD) greater than  $50 \mu\text{m}$  in diameter were forecast to exist. The majority of the research flights were directed into the warm-frontal regions of winter storms, and approximately 23 000 km of in-cloud measurements were obtained. Numerous observations of liquid, mixed, and glaciated cloud conditions made the dataset well suited for assessing instrument responses under all three kinds of conditions.

## 3. Instrumentation

Instrumentation mounted on the Convair-580 aircraft during CFDE I and III has been described in Isaac et al. (1998). Table 1 shows the instrumentation relevant to this investigation. The instruments were mounted on three underwing pylons, including a dedicated pylon for the LWC probes and two pylons that could each hold four PMS-type probes. The King LWC and Nevzorov LWC and total water content (TWC) instruments were all mounted on the LWC pylon, which also included a Sensor Systems, Goodrich Corporation, Rosemount temperature probe and a Pitot tube (Cober et al. 2001). The Nevzorov TWC probe measures the sum of LWC and IWC. The LWC pylon was situated to hold the instruments ahead of the leading edge of the wing to minimize flow effects associated with airflow around the wing. Flow effects were calculated following the method of Drummond and MacPherson (1985), and the correction factors for all of the LWC measurements were determined to be between 1.03 and 1.05. Flow corrections for the PMS FSSP and 2D probes (King 1986) were not accounted for, because the measurement biases associated with the flow fields (approximately 2%) were significantly less than the probe measurement accuracies ( $>15\%$ ).

The two PMS King probes (King et al. 1978) were calibrated in a high-speed wind tunnel by King et al. (1985) and were found to measure LWC to within

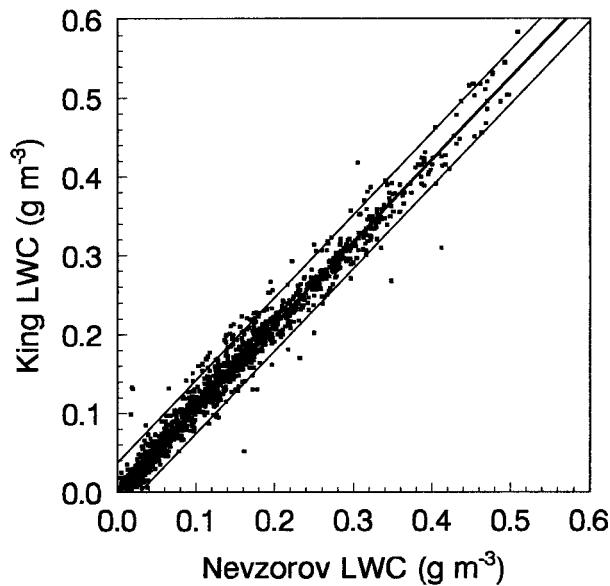


FIG. 1. Scatterplot of King LWC vs Nevzorov LWC for 30-s-averaged data. The data were taken from clouds with maximum droplet diameters  $<95 \mu\text{m}$  and negligible ice-crystal concentrations. The best-fit curve is shown along with curves that represent the 95% confidence interval (2 standard errors =  $\pm 0.034 \text{ g m}^{-3}$ ).

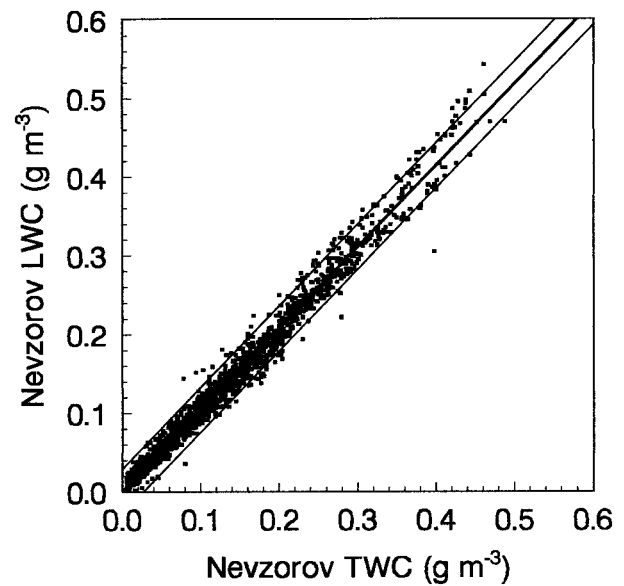


FIG. 2. Scatterplot of Nevzorov LWC vs Nevzorov TWC for 30-s-averaged data. The data were taken from clouds with maximum droplet diameters  $<95 \mu\text{m}$  and negligible ice-crystal concentrations. The Nevzorov TWC measurement is a measure of LWC in these cases. The best-fit curve and 95% confidence interval ( $\pm 0.028 \text{ g m}^{-3}$ ) are also shown.

$\pm 15\%$ , as compared with icing cylinders. Subsequent calibrations as discussed by Cober et al. (1995) and Strapp et al. (2000) have shown that the instruments remained stable over a long period of time and continued to measure LWC to within  $\pm 15\%$ . The dry power term was removed in a similar manner to that discussed by King et al. (1978) and Cober et al. (1995), and the baseline drift was estimated to be less than  $0.02 \text{ g m}^{-3}$ . The data from each flight were carefully examined to ensure that the baseline drift did not exceed  $0.02 \text{ g m}^{-3}$ , and poor data regions were identified and screened out. The instrument response to ice crystals will be discussed in section 4.

The Nevzorov LWC and TWC probes have been discussed by Korolev et al. (1998b). Comparisons with icing cylinders and King probe measurements in high-speed wind-tunnel experiments showed that the instruments were capable of measuring LWC and TWC, respectively, to within 15% with a sensitivity of  $0.003\text{--}0.005 \text{ g m}^{-3}$ . During the research flights, the Nevzorov zero levels were constantly adjusted to minimize baseline drift. During the postproject analysis, the Nevzorov data were examined further to remove any errors associated with baseline drift.

Figure 1 shows a comparison of the King LWC and Nevzorov LWC measurements for cloud conditions observed during CFDE I and III in which the maximum droplets observed with the FSSP were less than  $95 \mu\text{m}$  in diameter, the FSSP median volume diameter (MVD) was less than  $40 \mu\text{m}$ , and the ice-particle concentrations measured with the 2D probes were less than  $0.1 \text{ L}^{-1}$ . The maximum drop size and MVD were selected to

minimize the significant response falloff for large drops that affects both instruments (Biter et al. 1987, Strapp et al. 2000). IWC in these cases was negligible in comparison with LWC. Each data point represents an average over 30 s during which the aircraft was assessed to be in cloud. The two instruments show excellent agreement, with a standard error of  $0.017 \text{ g m}^{-3}$  and a correlation coefficient of 0.99. The best-fit curve has a slope of 1.04, with the King probe measuring slightly higher than the Nevzorov probe. This result is consistent with the observations of Korolev et al. (1998b). Points at which the two instruments showed a substantial difference were normally associated with periods when one of the instrument baselines was likely to have been offset from zero. The 95% confidence interval (2 standard errors) curves are also shown in Fig. 1. Figure 2 shows a comparison between the Nevzorov LWC and TWC measurements for the same cloud conditions described in Fig. 1. In clouds with negligible IWC, the TWC probe provides an additional measurement of the LWC. The best-fit curve has a slope of 1.03, with a standard error of  $0.014 \text{ g m}^{-3}$  and a correlation coefficient of 0.99. The excellent agreement is a reflection of the quality of the identification of the baseline, the close proximity of the two measurements, and the similarity of the measurement techniques.

The FSSP instruments were frequently calibrated with glass beads during the field projects, and the data were processed following the method of Cober et al. (1995). Particle concentrations were corrected for deadtime coincidence following the method of Baumgardner et al.

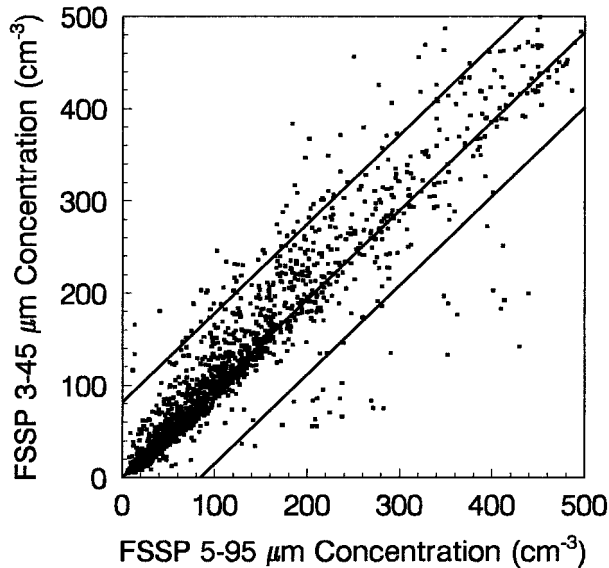


FIG. 3. Scatterplot of concentrations for the FSSP 3–45- $\mu\text{m}$  and FSSP 5–95- $\mu\text{m}$  instruments. The data represent 30-s averages. The data were taken from clouds with maximum droplet diameters  $<95\ \mu\text{m}$  and negligible ice-crystal concentrations. The best-fit curve and 95% confidence interval ( $\pm 82\ \text{cm}^{-3}$ ) are also shown.

(1985). Regions of bad data that were clearly caused by excessive ice buildup or fogging were manually identified and were removed from the dataset. Figure 3 shows a comparison of concentrations from the FSSP 3–45- $\mu\text{m}$  and FSSP 5–95- $\mu\text{m}$  probes for the same cloud conditions described in Fig. 1. The best fit has a slope of 0.97, with a standard error of  $41\ \text{cm}^{-3}$  and a correlation coefficient of 0.94. The concentration measurements show good agreement, but the relative error and scatter are higher than expected. Baumgardner (1983) estimated that a properly calibrated and corrected FSSP could provide concentration measurements to within  $\pm 17\%$ , so that two FSSPs should agree to within  $\pm 24\%$ . For the FSSP data shown in Fig. 3 and for concentrations greater than  $40\ \text{cm}^{-3}$ , only 77% of the data agreed to within the expected  $\pm 24\%$ . The discrepancies were likely caused by the following effects.

- 1) *The accumulation of ice on the FSSP.* Under some of the heavier icing conditions observed, the buildup of ice on the FSSP could distort the airflow into the sample area.
- 2) *Partial fogging of the instruments caused by changes in altitude.* Continuous ascents and descents were common in the majority of the research flights. The aircraft ascent and descent rates were limited to  $300\ \text{m}\ \text{min}^{-1}$  to minimize fogging; however, it was still observed on some occasions.
- 3) *Changing cleanliness of the optics from day to day.* The optics were cleaned every few flights, not after every flight.
- 4) *Unaccounted-for flow effects, as described by King (1986).* The two FSSPs were mounted in different

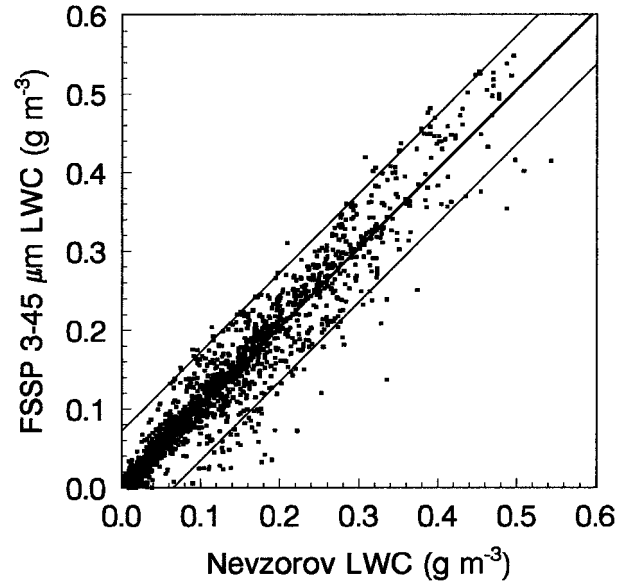


FIG. 4. Scatterplot of FSSP 3–45- $\mu\text{m}$  LWC vs Nevzorov LWC for 30-s-averaged data. The data were taken from clouds with maximum droplet diameters  $<95\ \mu\text{m}$  and negligible ice-crystal concentrations. The best-fit curve and 95% confidence interval ( $\pm 0.068\ \text{g}\ \text{m}^{-3}$ ) are also shown.

locations relative to the wing and hence would experience different errors associated with this effect.

- 5) *Ice-crystal contamination of the FSSP spectra.* This effect is expected to be minimized for the cases selected for the FSSP comparison because of the careful selection process used in identifying liquid-phase cases.

Figure 4 shows a comparison of the FSSP 3–45- $\mu\text{m}$  LWC versus the Nevzorov LWC. The best fit has a slope of 1.01, with a standard error of  $0.034\ \text{g}\ \text{m}^{-3}$  and a correlation coefficient of 0.95. This result suggests that there was no systematic bias between the LWC measurements. These results are consistent with the error estimates of Baumgardner (1983). Data points for which the FSSP significantly underestimates the LWC relative to the Nevzorov LWC could be caused by fogging of the FSSP. A comparison of the FSSP 5–95- $\mu\text{m}$  LWC versus the Nevzorov LWC showed similar results, with a best fit of 1.06 and standard error of  $0.07\ \text{g}\ \text{m}^{-3}$ . The FSSP 5–95- $\mu\text{m}$  data showed considerably more scatter than the FSSP 3–45- $\mu\text{m}$  data did, when compared with the Nevzorov LWC measurements. Although the scatter in the concentration data is larger than suggested by Baumgardner (1983), the good correlation between the two FSSP instruments combined with only small biases in the LWC correlations suggests that the instruments were working correctly and that the data are acceptable for use, albeit with a scatter that is somewhat larger than expected.

The data shown in Figs. 1 through 4 demonstrate two important points. First, the good agreements between

the instruments provide confidence in the measurements, which presumably can be applied to the remainder of the dataset. Second, because these data were screened to include only liquid-phase conditions with no large drops and no significant concentrations of ice crystals, the results are indicative of how the instruments are expected to respond under liquid-phase conditions. Different responses under mixed or glaciated conditions might allow techniques to be developed that can segregate these conditions. In contrast, similar responses under mixed or glaciated conditions might lead to a conclusion that phase segregation cannot be assessed with these instruments.

The three 2D probes listed in Table 1 were used to provide shape, size, and concentrations for particles within their respective size ranges. The first four channels of each 2D probe were ignored because of the depth-of-field and sizing uncertainties that exist for these channels (Korolev et al. 1998a; Joe and List 1987). Strapp et al. (2001) showed that distribution measurement errors for the PMS 2D-C monoscale probe, when expressed as sizing errors, were less than 10% for particles greater than or equal to 5 pixels (125  $\mu\text{m}$ ). The data from the PMS 2D-C grayscale probe were processed using two shadow levels (approximately 40%–50%), simulating a 2D-C monoscale probe response, although with a smaller sample volume.

#### 4. Instrument responses

##### a. Rosemount icing detector

A Rosemount icing detector (RID) model 871FA221B, manufactured by Sensor Systems, Goodrich Corporation, was mounted on the Convair-580 for all research flights made during CFDE I and III. The RID is a very useful instrument for segregating glaciated and nonglaciated conditions because it has no significant response to ice crystals. Heymsfield and Miloshevich (1989) showed that the 1-s response of their instrument to ice particles was less than 3  $\text{mV s}^{-1}$  for measurements made in cirrus clouds at temperatures less than  $-40^{\circ}\text{C}$ . Cober et al. (2001) used 30-s-averaged observations in midlatitude winter storms to show that the instrument response to ice particles was less than 2  $\text{mV s}^{-1}$  in 98.5% of the glaciated clouds observed. They identified regions of glaciated clouds using conservative interpretations of measurements from the 2D probes, Nevzorov LWC and TWC probes, and FSSP measurements. They also found that 99.6% of the average RID responses in clear air were less than 2  $\text{mV s}^{-1}$  and concluded that 30-s-averaged RID measurements made in clear air and glaciated clouds were indistinguishable. For an aircraft flying at 100  $\text{m s}^{-1}$ , which is the characteristic speed of the Convair-580, a 2  $\text{mV s}^{-1}$  signal would correspond to an LWC of approximately 0.002  $\text{g m}^{-3}$  (Cober et al. 2001). This value is at or below the minimum LWC threshold for the instrument. The LWC threshold is the

LWC for which sublimation balances accretion. Sublimation can occur in a water-saturated environment because of the adiabatic heating associated with the speed of the aircraft. The LWC threshold was estimated to be  $0.007 \pm 0.010 \text{ g m}^{-3}$  by Cober et al. (2001) and was theoretically predicted to be between 0.002 to 0.006  $\text{g m}^{-3}$  by Mazin et al. (2001) for an airplane flying at 100  $\text{m s}^{-1}$ . In mixed-phase conditions, Cober et al. (2001) found that the RID correlation with LWC was the same as for liquid-phase conditions, implying that the ice crystals neither accumulated to the sensing cylinder nor eroded the ice buildup to a measurable degree. Cober et al. (2001) concluded that for data averaged at 30-s resolution, glaciated cloud conditions could be inferred when the average RID signal was less than 2  $\text{mV s}^{-1}$  at temperatures less than  $-5^{\circ}\text{C}$ . A limitation of the RID is that the combination of dynamic heating and latent heat release from supercooled droplets that are freezing to the sensing cylinder can cause the ice surface temperature to reach  $0^{\circ}\text{C}$  (Ludlam 1951). The Ludlam limit is dependent on the air speed of the aircraft, LWC, and ambient temperature, and hence the instrument signal can be unreliable for combinations of LWC and temperature that cause the Ludlam limit to be reached (Baumgardner and Rodi 1989; Cober et al. 2001). When using the RID to identify glaciated conditions, care must be taken to ensure that the absence of a change in the voltage signal is not associated with an LWC that exceeded the Ludlam limit. In the CFDE dataset, such observations were infrequent at temperatures less than  $-4^{\circ}\text{C}$ . Therefore, the absence of a signal on the RID was used to infer glaciated conditions only for temperatures that were colder than  $-4^{\circ}\text{C}$ .

##### b. PMS 2D-C probes

The segregation of liquid and ice hydrometeors that are greater than or equal to 125  $\mu\text{m}$  (5 pixels) in diameter can be estimated using 2D images obtained from PMS 2D probes. The assumption is that circular images are usually interpreted as drops, whereas noncircular images are always interpreted as ice crystals. In either case, the particle must be imaged with adequate resolution to allow an assessment of the shape. In regions for which an insignificant quantity of the ice particles are apparently circular (i.e., frozen drops, small hexagonal plates, or heavily rimed ice crystals), statistics on the relative numbers of circles versus noncircles can be used to estimate the predominant particle phase. Cases with coexisting circular ice particles and supercooled large drops greater than or equal to 125  $\mu\text{m}$  were found to be infrequent enough that they did not affect the conclusions. This will be demonstrated below.

Particle images were processed following the center-in technique of Heymsfield and Parrish (1978). Particles that did not shadow an edge diode were assessed directly. Particles that shadowed an edge diode and had their center in the diode array were reconstructed by

assuming that the particle was a circle. Reconstruction involved reflecting the imaged portion of the particle through the line that intersected the particle center and adding some of the reflected portion to the original image until the reconstructed particle had an equal height and width. Several geometric ratios were applied to each 2D image to establish whether it was a circle or non-circle. Each ratio was designed so that the value would theoretically be equal to 1 for a circle. These ratios included the following:

$$\text{diameter ratio} = \frac{X + 1}{Y}, \quad (1)$$

$$\text{area ratio} = \frac{\pi(X + 1)Y}{4A}, \quad (2)$$

$$\text{perimeter ratio} = \frac{\pi\sqrt{(X + 1)^2 + Y^2}}{\sqrt{2}P}, \quad \text{and} \quad (3)$$

$$\text{perimeter-area ratio} = \frac{4A}{YP}, \quad (4)$$

where  $X$  is the particle width (size along the air speed motion direction) in pixels,  $Y$  is the height (size across the diode array),  $A$  is the area, and  $P$  is the perimeter. The area physically represents the number of shadowed pixels for a particle; the perimeter represents the total number of perimeter pixels. The perimeter was determined using a similar technique to that described by Korolev and Sussman (2000). One pixel is added to the  $X$  diameter to account for the first slice, which is not recorded, on the 2D-C and 2D-P mono probes. For 2D-C gray measurements, the first slice is recorded so that this correction was not required. The  $X$  and  $Y$  symmetry were also determined for each particle by overlaying an image with its reflection through the  $X$  or  $Y$  line, respectively, that intersected the center of the particle. The ratio of the number of overlapping pixels to the total number of pixels was used to quantify the symmetry. For a symmetrical particle, the  $X$  and  $Y$  symmetry would be 1 because the reflected particle would exactly overlap the original. In total, there were six geometric ratios that were determined for each particle. Theoretically, each ratio would be equal to 1 for a circular particle. However, because each 2D image was made up of a finite number of pixels, the actual values of the ratios for circular images bracketed the value 1.

Observations from warm clouds were used to determine the range of acceptable values for each geometric ratio. Clouds with temperatures greater than  $0^{\circ}\text{C}$  that had no ice crystals were selected, and all images, less artifacts, were extracted for the calibration dataset. Only images that were fully within the array (i.e., end-element rejection criterion) were used for the calibration. Figure 5 shows the maximum and minimum limits as a function of particle size for each geometric criterion for the 2D-C mono and 2D-C gray probes. A minimum of 100 measurements was required for each particle size for

the results shown in Fig. 5. The curves do not extend beyond 21 pixels for the 2D-C grayscale and 26 pixels for the 2D-C monoscale because insufficient observations at these sizes were collected. As expected, the curves tend to level off with increasing particle size while becoming increasingly discriminating and accurate at identifying circles. The geometric criteria at a particle size of 26 pixels for the 2D-C mono and 21 pixels for the 2D-C gray were used when assessing particles that were larger. This will introduce some error in identification of circles versus noncircles for these large particles, because of the greater restrictions associated with the larger diameters. The diameter ratio was forced to have a value greater than or equal to 1 by taking the inverse of Eq. 1 when the value is less than 1. The curve representing a geometric ratio of 1 in Figs. 5b,d represents the minimum possible diameter ratios and the maximum possible  $X$  and  $Y$  symmetry.

When processing the 2D measurements taken during CFDE I and III, several rejection criteria were applied to the data prior to testing whether a particle was a circle or noncircle. These rejection criteria included identification of zero-area images, minimum-diameter images, images with embedded blank slices in either the  $X$  or  $Y$  planes, out-of-focus images, and center not in images. Streaking images associated with ice buildup on and shedding off of the probe tips were also removed. The out-of-focus rejection criterion requires additional discussion. Oversizing of particles that are out of focus has been well documented (Korolev et al. 1998a; Strapp et al. 2001). This effect is particularly pronounced for particle sizes for which the depth of field is smaller than the distance between the probe arms. For the 2D-C mono and 2D-C gray instruments operated at  $25\text{-}\mu\text{m}$  resolution, this included all particles less than or equal to 7 pixels in diameter. Out-of-focus images are characterized by the existence of holes in the 2D images and were only observed in particles less than 10 pixels in diameter. Particles with holes at the center were rejected as being out of focus. Out-of-focus particles normally accounted for approximately 10% of the analyzed particle images. The out-of-focus screening removed both ice-crystal and drop images.

For an image to be assessed as a circle, it had to pass each of the six geometric tests. Noncircles would normally fail one or more tests. Using the entire CFDE I and III datasets and the phase assessment of liquid or glaciated (see section 5), the average fraction of circles for each particle size was assessed for liquid and glaciated clouds. The results for the 2D-C mono and 2D-C gray are shown in Fig. 6, which clearly illustrates the accuracy of the circular identification technique. In liquid clouds, for which the fraction of circles should be 1, the geometric criteria were able to identify 85%–95% of the 2D-C mono and  $>85\%$  of the 2D-C gray images as circles. Using geometric criteria at sizes larger than that at which the calibrations were determined caused some of the incorrect particle identifications. The finite

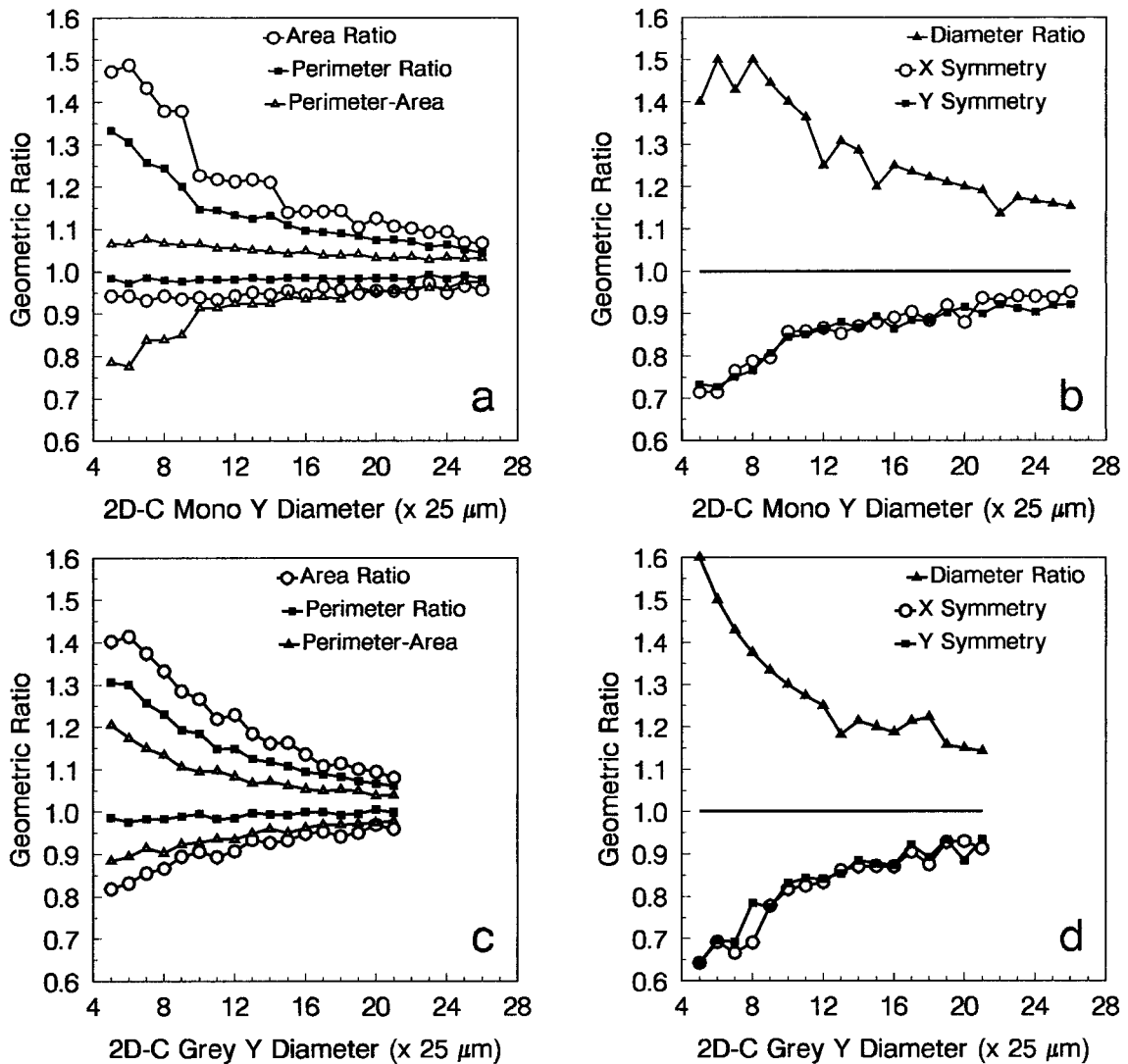


FIG. 5. Maximum and minimum geometric limits for circular images measured with the (a), (b) 2D-C mono and (c), (d) 2D-C gray probes for each geometric test as a function of particle height  $Y$ . These tests include area ratio, perimeter ratio, and perimeter–area ratio [(a) and (c)] and diameter ratio,  $X$  symmetry, and  $Y$  symmetry [(b) and (d)]. The geometric ratios for a given size were only determined when the number of calibration observations exceeded 100. The calibration curves were not determined for particles  $<5$  pixels in diameter. The curve representing a geometric ratio of 1 represents the minimum diameter ratio and maximum  $X$  and  $Y$  symmetry.

number of drops used in the calibrations caused additional error. For example, if only 100 calibration drops are used for a given diameter, then the maximum and minimum values observed for each geometric ratio represent approximately the 99th and 1st percentiles, respectively. This implies that 2% of drops will be rejected for each geometric criterion. With six criteria used to distinguish circles and assuming that each criterion is independent (which is not strictly correct), up to 12% of the circular images of the given diameter could be rejected in the subsequent analysis as a result of using only 100 drops for the calibrations. It would be ideal to use several thousand images to calibrate each particle size. These explanations account for the slight decrease in accuracy with increasing diameter in liquid-phase

clouds. For the glaciated-phase clouds, the identification of circular images changes significantly from 35% for 5–6 pixel particles to less than 10% for particles greater than 13 pixels in diameter. This implies that in mixed-phase clouds the errors in interpreting circular ice particles as liquid drops could be significant given that as many as 35% of the 6-pixel ice particles will be assessed as circular.

The CFDE I and III data were averaged at 30-s resolution. Using multiple instruments and the techniques summarized in section 5, the phase of each 30-s data point was assessed as liquid, mixed, or glaciated. For each data point, using all 2D images greater than or equal to 5 pixels in diameter, the ratio of circular or noncircular images to the total was determined. Figure

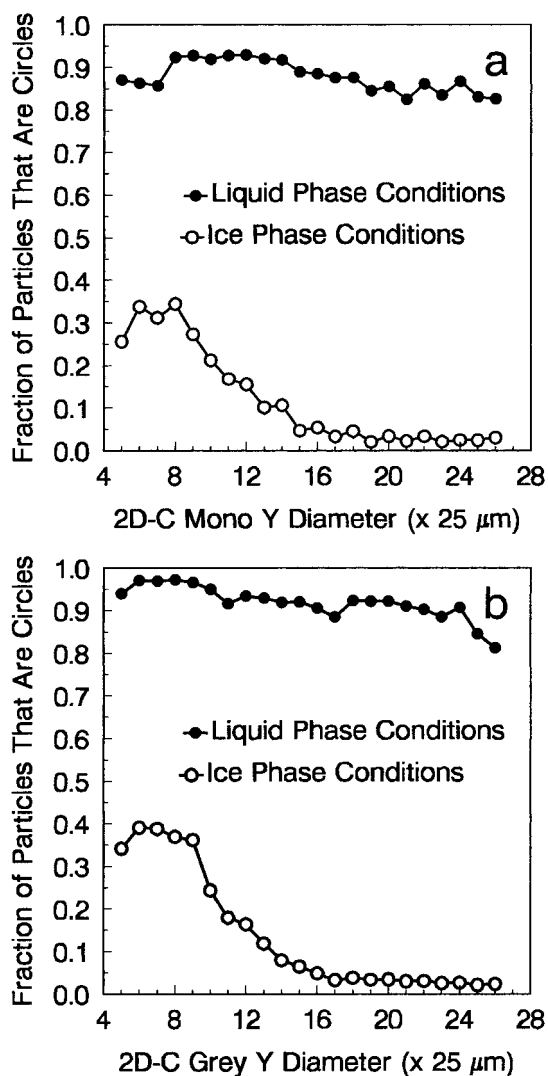


FIG. 6. Relative fractions of circular images observed in liquid and glaciated cloud conditions for the (a) 2D-C mono and (b) 2D-C gray probes, respectively, as a function of particle height  $Y$ . For a particle to be assessed as a circle, it had to pass each of the six geometric tests. These curves represent averages for the 2D-C mono and 2D-C gray probes for the entire CFDE-I and CFDE-III datasets. Only cloud cases that were assessed as being liquid or glaciated phase were used in these averages.

7 shows a histogram of these ratios for 1) liquid-phase clouds in which SLD greater than or equal to  $125 \mu\text{m}$  were observed, 2) glaciated-phase clouds in which no liquid drops were believed to exist, and 3) mixed-phase clouds in which ice crystals and SLD greater than or equal to  $125 \mu\text{m}$  were observed. Only data points with greater than 100 analyzed 2D particles are included in the data shown in Fig. 7. Most of the liquid-phase cases had an average circle ratio greater than 0.8, which is consistent with the maximum errors for the liquid-phase conditions assessed in Fig. 6. For glaciated conditions, the ratio of circles varied between 0.1 and 0.4, which is also consistent with the results in Fig. 6. The higher

number of 5–7-pixel particles versus larger particles will dominate the average fraction of noncircles for most of these cases. For mixed-phase cases, the ratio of circular images spanned all fractions, with a prominent peak around 0.3. The mixed-phase data with circular particle ratios less than 0.4 were primarily associated with cloud regions in which ice crystals and small supercooled cloud droplets coexisted. In these cases, circular ice crystals greater than or equal to  $125 \mu\text{m}$  may have been interpreted as liquid drops. The 2D images for each case were examined visually to confirm the analysis.

### c. Nevzorov LWC and King LWC probes

Glaciated cloud conditions at temperatures colder than  $-4^\circ\text{C}$  were identified using the RID and were confirmed by examining the 2D-C mono or 2D-C gray segregation of circles and noncircles. Figure 8a shows the response of the Nevzorov LWC and TWC probes for these conditions, as well as the response for the liquid-phase conditions from Fig. 2. The lower curve in Fig. 8a represents an LWC:TWC ratio of 0.25, with a small offset of  $0.01 \text{ g m}^{-3}$ . Because this ratio bounds most of the glaciated data, it might be used as a threshold for inferring glaciated conditions, except for TWC less than  $0.04 \text{ g m}^{-3}$ . Figure 8b shows the relative ratio of LWC:TWC for TWC greater than  $0.075 \text{ g m}^{-3}$  for glaciated-phase conditions. TWC measurements less than  $0.075 \text{ g m}^{-3}$  were not included to avoid any significant influence of baseline errors, which could be as high as  $0.02 \text{ g m}^{-3}$ . Figures 8c,d show similar results for the King probe. There are fewer data points for the King probe because it was not working on several flights. In glaciated clouds, the average LWC response is 19% of the IWC for the Nevzorov probe and 15% for the King probe. In general, the response to ice is similar for both instruments, although the King probe data show a larger scatter. Strapp et al. (1999) found that the Nevzorov and King LWC probes showed a 40% response to IWC in glaciated conditions. Their aircraft flew at  $200 \text{ m s}^{-1}$ , and the clouds they measured were primarily thunderstorm anvils with high concentrations of small ice particles. The fractional response of the hot-wire LWC instruments to ice crystals is probably dependent on the air speed of the research aircraft and the size of the ice crystals being measured (Strapp et al. 1999). This is likely a partial explanation for the scatter shown in Figs. 8b,d. Although Cober et al. (1995) and Korolev et al. (1998b) discussed the response of the hot-wire LWC probes to ice crystals, neither of these studies quantified the false response of the LWC probes in glaciated clouds using a large dataset. On average, for the CFDE dataset, 15%–20% of the ice water content was reflected as a false LWC on the Nevzorov and King LWC probes. Therefore, when assessing mixed-phase conditions, the hot-wire LWC and TWC measurements can be used to derive the cloud LWC and IWC as

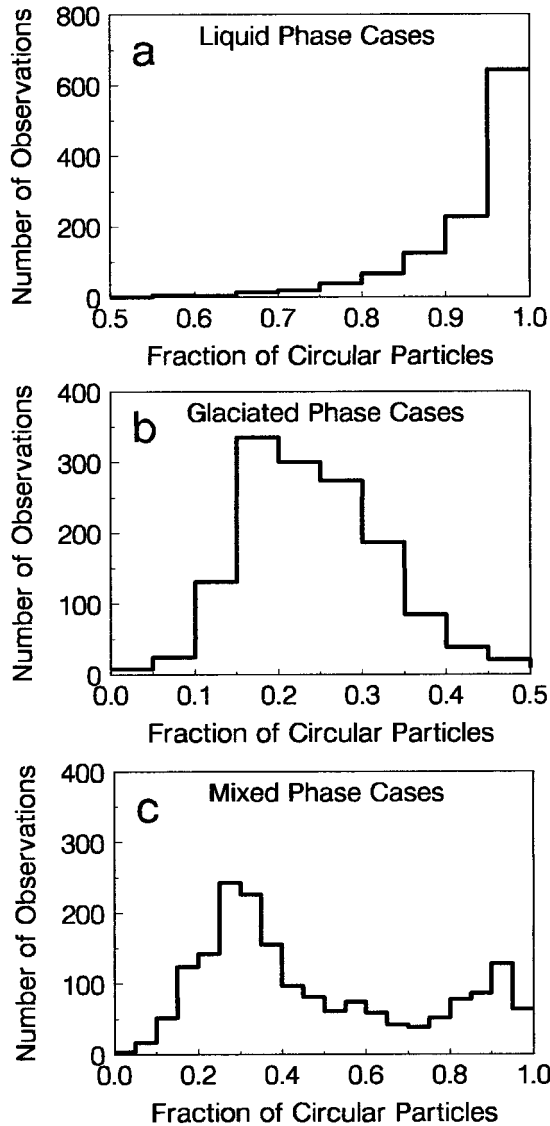


FIG. 7. Histograms of the fractions of circular images for (a) liquid-phase cases with drops  $\geq 125 \mu\text{m}$ , (b) glaciated-phase cases with no LWC or drops  $\geq 125 \mu\text{m}$ , and (c) mixed-phase cases with ice crystals and drops  $\geq 125 \mu\text{m}$  in diameter. Each observation represents a 30-s average for which a minimum of 100 2D images was assessed with the geometric criteria discussed in section 4.

$$\text{Nevzorov TWC} = \text{LWC} + \text{IWC}, \quad \text{and} \quad (5)$$

$$\begin{aligned} \text{Nevzorov or King LWC} = \text{LWC} \\ + (0.15 \pm 0.10)\text{IWC}. \end{aligned} \quad (6)$$

*d. PMS FSSP probes*

Gardiner and Hallett (1985) showed that ice crystals were detected by the FSSP at concentrations 2–3 orders of magnitude larger than the ice-crystal concentrations inferred from 2D-C and replicator probes. They also showed that the ice crystals would primarily cause

counts in the higher FSSP channels. This would cause the FSSP to measure an apparent high MVD or mean diameter in glaciated cloud conditions. To examine the effects of ice crystals on the FSSP spectra observed during CFDE I and III, the RID, Nevzorov LWC and TWC probes, and 2D measurements were used to segregate the data into liquid-, mixed-, and glaciated-phase cases. To ensure the usefulness of the RID, only data at temperatures less than  $-4^\circ\text{C}$  were used for the following discussion. Glaciated cases were assumed for RID less than  $2 \text{ mV s}^{-1}$ , Nevzorov LWC:TWC fraction less than 0.25, fraction of noncircular 2D images greater than 0.6, and visual assessment that the 2D images appeared to be primarily ice crystals. Liquid conditions were assumed for RID greater than  $2 \text{ mV s}^{-1}$ , agreement between the Nevzorov LWC and TWC probes within 15%, concentrations of ice crystals less than  $0.1 \text{ L}^{-1}$  as measured with the 2D probes, and visual confirmation that there were very few or no ice crystals in the 2D data. Cases with significant mass in drizzle sizes, for which the Nevzorov LWC and TWC did not agree within 15% because of the falloff of the LWC probe (Biter et al. 1987; Strapp et al. 2000), were assessed as liquid if the fraction of circular 2D images was greater than 0.85 and visual assessment of the 2D data confirmed there were very few or no ice crystal images (approximately 10% of the liquid-phase cases). Mixed-phase cases were assessed for Nevzorov LWC:TWC between 0.25 and 1.0, visual identification of ice crystals in the 2D imagery, and RID greater than  $2 \text{ mV s}^{-1}$ . The FSSP data were separately averaged for all liquid, mixed, and glaciated cloud regions observed during CFDE I and III. Figure 9a shows the normalized LWC for the average liquid and glaciated spectra measured with the two FSSPs on the 5–95- $\mu\text{m}$  and 3–45- $\mu\text{m}$  ranges, respectively. The LWC was derived assuming that the measured spectra were composed of liquid water drops. The liquid and glaciated spectra intersect around channel 6 (38  $\mu\text{m}$ ) on the 5–95- $\mu\text{m}$  range and channel 11 (33  $\mu\text{m}$ ) on the 3–45- $\mu\text{m}$  range. The glaciated spectrum drops off rapidly for decreasing sizes, implying that, for measurements made in mixed-phase conditions, ice crystals in winter clouds similar to those observed during CFDE would not significantly contaminate the lower FSSP channels. In these cases, the lower FSSP channels would presumably be dominated by droplets. Ice crystals would dominate the spectrum for larger channels. The ice-crystal concentrations  $C$  measured with the 2D probes ( $\geq 125 \mu\text{m}$ ) were used to segregate the mixed-phase conditions into four categories including  $0 \leq C < 1 \text{ L}^{-1}$ ,  $1 \leq C < 5 \text{ L}^{-1}$ ,  $5 \leq C < 10 \text{ L}^{-1}$ , and  $C > 10 \text{ L}^{-1}$ . The data averaged over all CFDE I and III observations are shown in Figs. 9b–d for three different FSSP ranges including 5–95, 3–45, and 2–31  $\mu\text{m}$ , respectively. The liquid and glaciated curves for the 5–95- and 3–45- $\mu\text{m}$  ranges shown in Fig. 9a are the same as those in Figs. 9b,c, respectively. It is clear in Figs. 9b,c that, as the ice-crystal concentration increases, the

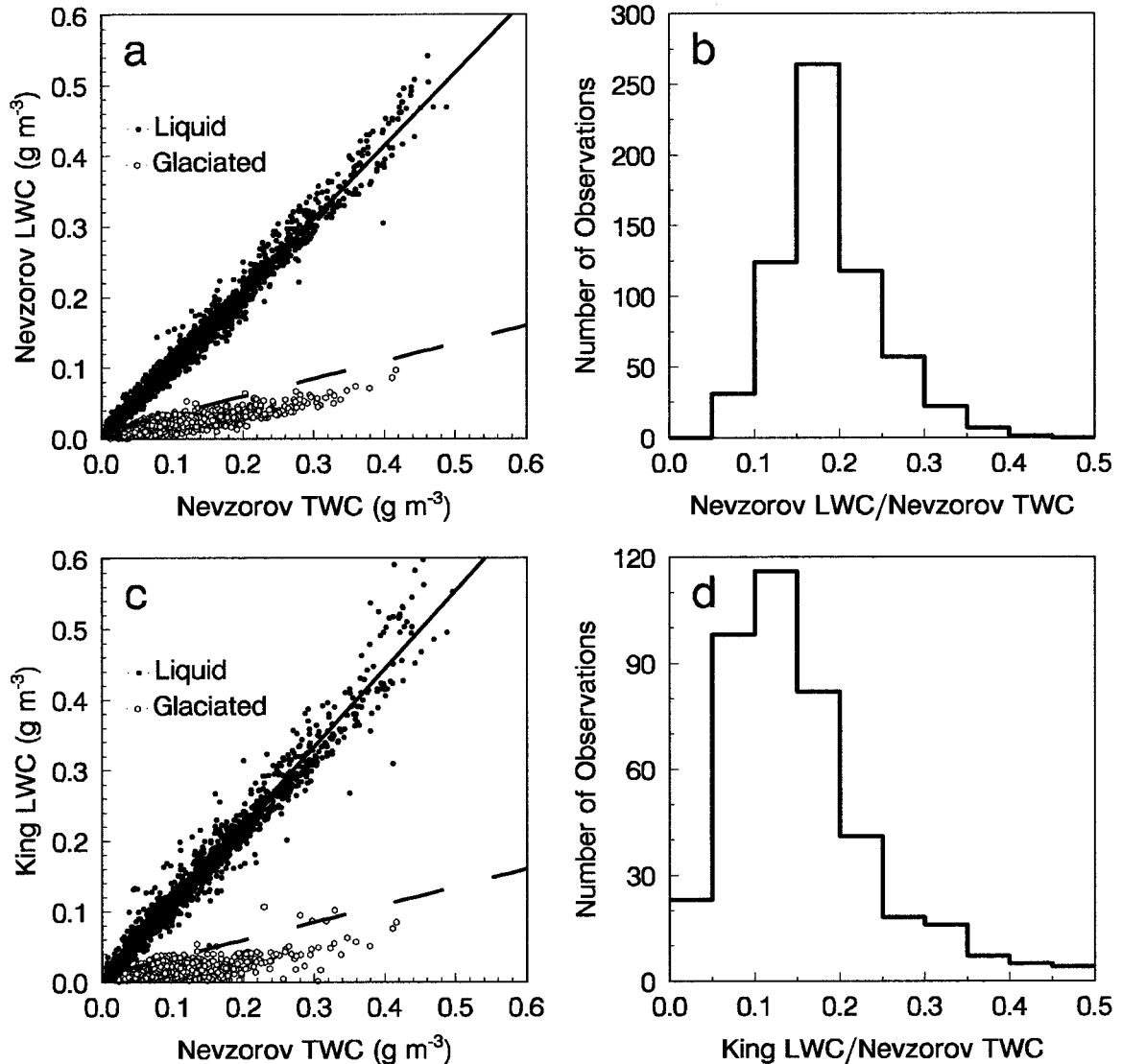


FIG. 8. (a) Scatterplot of Nevzorov LWC vs Nevzorov TWC for liquid (1723 observations) and glaciated (825 observations) conditions; (b) histogram of the ratio of LWC:TWC for the Nevzorov LWC probe for glaciated cloud cases for which the TWC = IWC and TWC > 0.075 g m<sup>-3</sup>; (c) scatterplot of King LWC vs Nevzorov TWC for liquid (1529 observations) and glaciated (531 observations) conditions; (d) histogram of the ratio of LWC:TWC for the King LWC probe for glaciated cloud cases for which the TWC = IWC and TWC > 0.075 g m<sup>-3</sup>. For (a) and (c), the best fits for the liquid-phase cases are shown, as are curves representing LWC:TWC = 0.25. The latter curves represent a suitable threshold for segregating glaciated conditions.

average mixed-phase spectrum for sizes greater than 35  $\mu\text{m}$  evolves from the average liquid-phase spectrum to the average glaciated-phase spectrum. For  $C$  less than  $1 \text{ L}^{-1}$ , the spectrum is essentially the same as the average liquid-phase spectrum, implying minimum contamination of the droplet spectrum measured on the FSSP. Conversely, for  $C$  greater than  $10 \text{ L}^{-1}$ , the curve is similar to the average glaciated-phase spectrum curve, implying that ice crystals are dominating the FSSP spectrum for sizes larger than 35  $\mu\text{m}$ . The curve for  $1 \leq C < 5 \text{ L}^{-1}$  is also contaminated by ice crystals for sizes above 35  $\mu\text{m}$ . All four mixed-phase curves, on each range, show a characteristic mode for droplets less than

25  $\mu\text{m}$ . Similar results were observed when the mixed-phase data were segregated by ice water fraction, with ice water fractions less than 0.2 showing minimal crystal contamination of the FSSP spectrum. Figure 9d demonstrates that, in mixed-phase conditions, regardless of the ice-crystal concentrations observed, the average FSSP spectrum for sizes less than 31  $\mu\text{m}$  was dominated by the droplet spectrum and the artifacts associated with ice crystals did not affect the measurements of the droplet spectrum. These observations may not always hold for individual 30-s cases. For example, measurements of drizzle collected below cloud base could have an FSSP spectrum similar to the average glaciated spec-

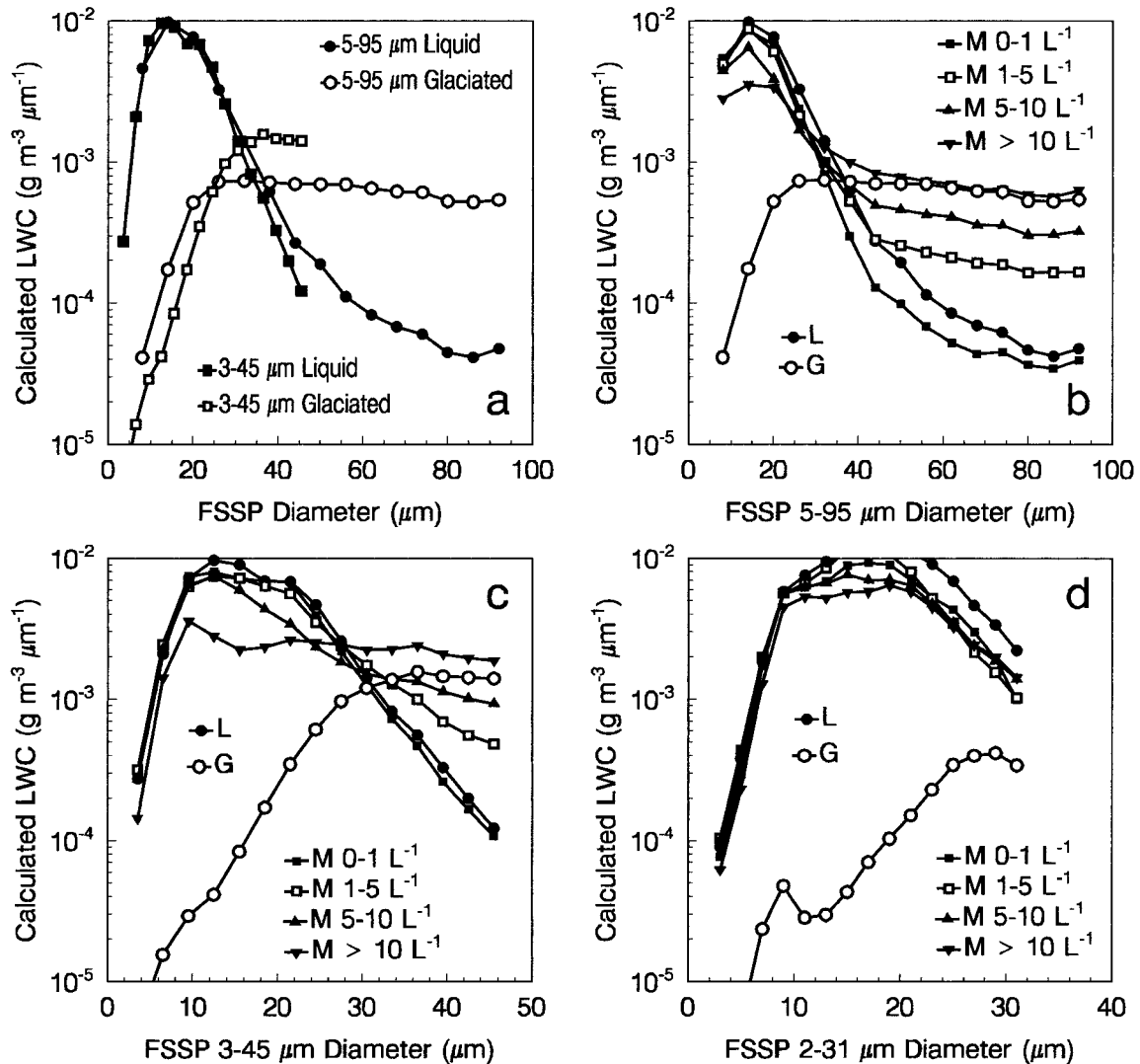


FIG. 9. (a) Average particle mass spectra for the collective CFDE-I and -III dataset for the 5–95- $\mu\text{m}$  and 3–45- $\mu\text{m}$  FSSP probes operated on these ranges. The data are segregated into liquid and glaciated conditions. (b) Average particle mass spectra for the FSSP 5–95- $\mu\text{m}$  probe operated on the 5–95- $\mu\text{m}$  range. The data are segregated into liquid (L), mixed (M), and glaciated (G) conditions. The mixed-phase cases are segregated by ice-crystal concentration, for crystals  $\geq 125 \mu\text{m}$  as measured with the 2D probes. (c) Average particle mass spectra for the FSSP 3–45- $\mu\text{m}$  probe operated on the 3–45- $\mu\text{m}$  range. The data are segregated as in (b). (d) Average particle mass spectra for the FSSP 3–45- $\mu\text{m}$  probe operated on the 2–31- $\mu\text{m}$  range. The data are segregated as in (b).

trum. This illustrates the necessity to use multiple instruments when assessing cloud phase.

Although the response of the FSSP will depend somewhat on the actual ice-crystal distribution, the results in Fig. 9 demonstrate that, when the data are averaged over a large dataset, very specific trends are apparent. The average responses of the FSSPs to ice-crystal spectra in midlatitude winter clouds were observed to be extremely consistent from flight to flight and from project to project. These responses can clearly be segregated from the response to liquid clouds. These results do not demonstrate that FSSP measurements in mixed and glaciated clouds are useful, only that they can be used to help to identify the cloud phase and hence set

an upper bound on what part of the FSSP spectrum can be used for droplet measurements.

Gardiner and Hallett (1985) showed that FSSP-measured concentrations in glaciated clouds were 100 to 1000 times greater than the ice-crystal concentrations measured with a formvar replicator and 2D-C probe. Similar for the CFDE data, the FSSP-measured concentrations in glaciated clouds were between 10 and 500 times greater than the ice-crystal concentrations ( $\geq 125 \mu\text{m}$ ) measured with a 2D-C probe. The absence of an RID signal implies that the LWC is less than  $0.01 \text{ g m}^{-3}$  for these cases, so it is unlikely that the differences in the FSSP and 2D-C concentrations are caused by small cloud droplets. Gardiner and Hallett (1985) believed that

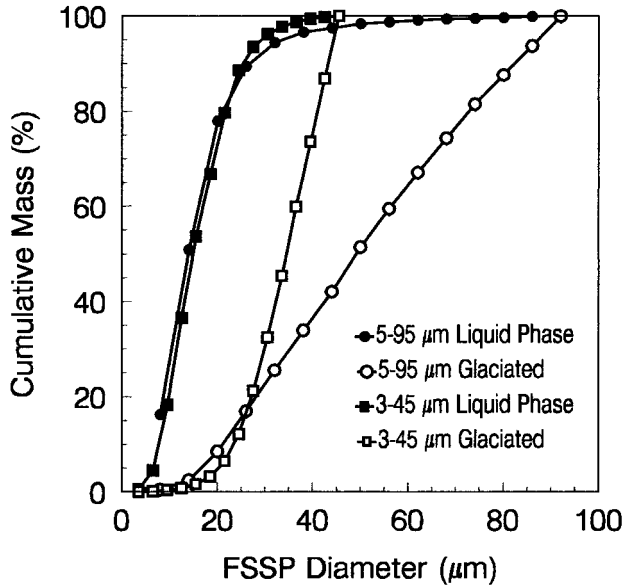


FIG. 10. Cumulative mass distributions for the average liquid and glaciated spectra measured with the FSSP 5-95- $\mu\text{m}$  and FSSP 3-45- $\mu\text{m}$  probes (Fig. 9a). The data represent the average liquid and glaciated spectra for the entire CFDE-I and -III datasets.

the exaggerated FSSP concentrations were not caused by small ice particles that had been missed by their 2D and replicator instruments as a result of optical or collision efficiency effects. However, because the 2D measurements here have been truncated at 125, it is possible that ice crystals less than 125  $\mu\text{m}$  in diameter could account for some or all of the differences in the 2D and FSSP concentrations.

Figure 10 shows the cumulative mass plots for the same data shown in Fig. 9a. These were computed by assuming that the observed FSSP spectra were liquid spherical particles. For glaciated conditions, this is not the case and the cumulative mass will not be representative of the actual spectra. The significant difference in MVD (50% mass diameter) between the liquid and glaciated averages, especially for the 5-95- $\mu\text{m}$  range, suggests that the calculated MVD could be a useful tool for identifying glaciated conditions. Figure 11 shows a histogram of the MVD values observed for the 30-s-averaged data for liquid, mixed, and glaciated conditions for the 5-95- $\mu\text{m}$  and 3-45- $\mu\text{m}$  probes. For the 5-95- $\mu\text{m}$  probe, MVD values greater than 30  $\mu\text{m}$  accounted for 792 out of 793 of the glaciated-cloud cases and 23 out of 626 (4%) of the liquid-cloud cases observed. The results for the 3-45- $\mu\text{m}$  probe were similar, with MVD greater than 30  $\mu\text{m}$  accounting for 375 out of 375 glaciated cases and 5 out of 334 (2%) of the liquid-phase cases. Using the 80% mass diameter (80VD) rather than the 50% mass diameter (MVD) allows for a clearer segregation of the liquid and glaciated cases. An 80VD greater than 40  $\mu\text{m}$  accounts for 14 out of 626 (2%) of the liquid cases and 793 out of 793 (100%) of the glaciated cases. Concentrations measured with the 5-95-

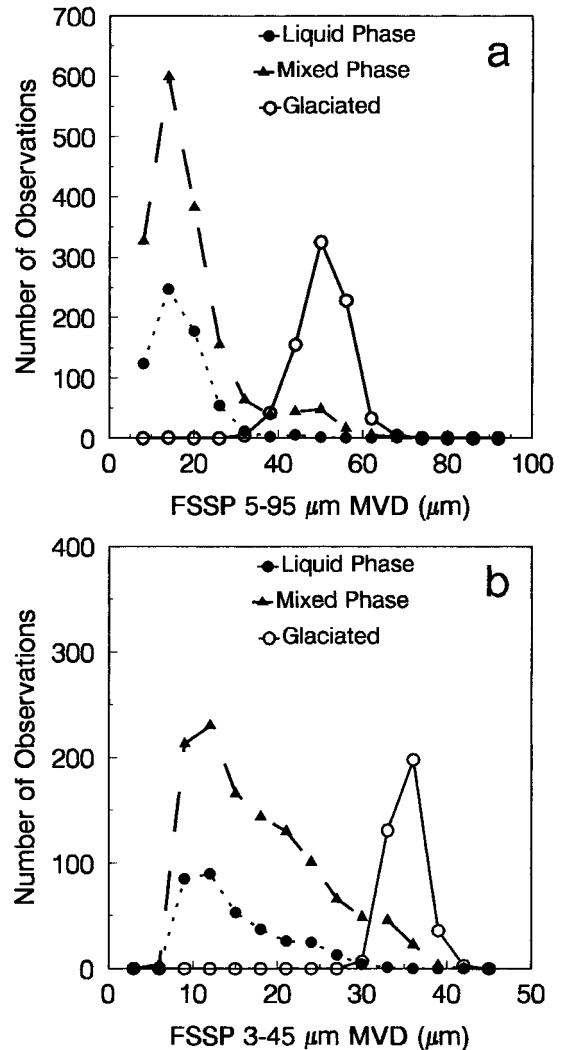


FIG. 11. Histogram of the 50% mass diameters (MVD) for liquid, mixed, and glaciated conditions for (a) 5-95- $\mu\text{m}$  FSSP and (b) 3-45- $\mu\text{m}$  FSSP. Each observation represents a 30-s average. The instruments were used on the 5-95- and 3-45- $\mu\text{m}$  ranges, respectively.

$\mu\text{m}$  and 3-45- $\mu\text{m}$  probes were less than 15  $\text{cm}^{-3}$  for all glaciated clouds and for 8% of the liquid-phase clouds observed. The histogram of mixed-phase conditions in Fig. 11 showed overlap with the liquid and glaciated curves, although it generally followed the liquid-phase trends. These results indicate that FSSP spectra can be used in this dataset to segregate the majority of observations into nonglaciated-phase or nonliquid-phase categories. Other instruments will allow additional segregation of mixed-phase conditions from the liquid and glaciated observations.

## 5. Phase estimation

For the previous analysis, cloud phase was identified only for regions in which the temperature was less than  $-4^{\circ}\text{C}$  in order to have confidence in the RID results.

TABLE 2. Summary of the observed instrument responses for each cloud phase.

Parameter	Liquid phase	Glaciated phase	Mixed phase	Notes
Nevzorov LWC:TWC	>0.85	<0.25	0.25–1.0	<0.85 with drizzle
King LWC:TWC	>0.85	<0.25	0.25–1.0	<0.85 with drizzle
2D-C mono circle fraction	>0.85	<0.35		Sizes $\geq 5$ pixels
2D-C gray circle fraction	>0.85	<0.40		Sizes $\geq 5$ pixels
FSSP MVD 5–95 $\mu\text{m}$		>30 $\mu\text{m}$		4% of liquid cases
FSSP 80VD 5–95 $\mu\text{m}$		>40 $\mu\text{m}$		2% of liquid cases
FSSP concentration		<15 $\text{cm}^{-3}$		8% of liquid cases
Rosemount icing detector	>2 $\text{mV s}^{-1}$	<2 $\text{mV s}^{-1}$	>2 $\text{mV s}^{-1}$	Temperature < $-4^{\circ}\text{C}$

Each instrument was assessed in liquid and glaciated conditions to differentiate characteristic responses for each kind of condition. A summary of the instrument responses is listed in Table 2. By following Table 2, liquid-phase clouds can be assessed for temperatures less than  $-4^{\circ}\text{C}$  when the following conditions are met: agreement between the Nevzorov LWC and TWC probes is within 15%, fraction of circular particles measured with the 2D probes is greater than 0.85, RID is greater than  $2 \text{ mV s}^{-1}$ , and visual assessment shows very few or no ice crystals in the 2D imagery. For cases in which the 2D data showed no particles greater than or equal to  $125 \mu\text{m}$ , the cloud was assumed to have no significant IWC. This is a reasonable assumption for the midlatitude winter clouds observed during CFDE I and III, in which the temperatures and vapor pressures would cause at least some of the ice crystals to grow rapidly to sizes greater than  $100 \mu\text{m}$  in diameter. For cases with significant drizzle concentrations, the LWC:TWC fraction was not expected to agree within 15%. In a similar way, Table 2 shows that glaciated cloud conditions at temperatures less than  $-4^{\circ}\text{C}$  can be assessed under the following conditions: fraction of circular images on the 2D probes less than 0.35, Nevzorov LWC:TWC fraction less than 0.25, FSSP concentrations less than  $15 \text{ cm}^{-3}$ , RID less than  $2 \text{ mV s}^{-1}$ , and FSSP MVD greater than  $30 \mu\text{m}$ . Assessment of mixed-phase cases at temperatures less than  $-4^{\circ}\text{C}$  required RID greater than  $2 \text{ mV s}^{-1}$ , Nevzorov LWC:TWC fractions between 0.25 and 1.0, and visual assessment of ice crystals in the 2D imagery. The results in Table 2 are based on analysis of data averaged at 30-s resolution. This averaging period was selected to ensure that there were sufficient 2D images ( $>100$ ) for the majority of data points. No changes in the results were observed for longer averaging intervals. However, for shorter averaging intervals, the 2D and FSSP spectra showed greater variability, and hence the results in Table 2 should be used subjectively.

In the absence of an RID measurement or at temperatures greater than  $-4^{\circ}\text{C}$  for which the RID measurements were considered to be unreliable for the CFDE data, the conditions listed in Table 2 can be applied to estimate the cloud phase. When these criteria were applied to the 30-s-averaged CFDE data with temperatures between  $0^{\circ}$  and  $-4^{\circ}\text{C}$ , they identified 177 gla-

ciated-, 441 liquid-, and 645 mixed-phase cases out of a total of 1535 observations, accounting for 82% of this data. There were two primary reasons why 18% of these data did not meet any of the screening criteria including 1) insufficient 2D particles for using the 2D assessment and 2) FSSP concentrations greater than  $15 \text{ cm}^{-3}$  in conditions that otherwise appeared to be glaciated and that had RID less than  $2 \text{ mV s}^{-1}$ . In the majority of the cases with small 2D concentrations, careful examinations of the data, including visual estimates of the particle habits, were performed prior to estimating the phase. For the cases that appeared glaciated but that had FSSP concentrations greater than  $15 \text{ cm}^{-3}$ , the FSSP data always indicated a small cloud mode of droplets less than  $20 \mu\text{m}$ , consistent with the mixed-phase conditions shown in Fig. 9. Hence, the phases of the remaining data were estimated after carefully examining the 2D spectra, the FSSP spectra, and the LWC measurements. This result demonstrates that the criteria listed in Table 2 may be useful for research aircraft that do not have an RID but do have the other instruments.

Some liquid-phase cases will contain an IWC that cannot be segregated from the TWC signal, because uncertainties of  $\pm 15\%$  between the LWC and TWC probes can mask a small IWC signal. In addition, some of the irregular images observed with the 2D probes in clouds that were assessed to be liquid phase may have been ice crystals. Considering that in liquid-phase clouds the geometric formulas incorrectly identify between 5% and 15% of the circular images as irregular, ice particles can be inherent in the 2D data for cloud regions that are classified as liquid phase. Shape recognition is not entirely habit recognition, and circular images are assumed to be drops in liquid-phase clouds. However, some of the circular images identified on the 2D probes may have been ice particles since, as was shown in section 4, between 5% and 40% of the ice particles in glaciated clouds will be identified as circular. To minimize these errors, the data were visually assessed and regions with obvious ice particles were identified. Cases with significant concentrations of drizzle drops and circular ice crystals were infrequent in the CFDE I and III dataset. It is estimated that any IWC inherent in the liquid-phase cases was less than 5% of the TWC for all the liquid-phase cases identified.

Some glaciated cases may contain a small LWC that

TABLE 3. Assessment of cloud phases observed for each project. Each observation represents a 30-s average during which the temperature is less than 0°C and TWC is greater than 0.01 g m<sup>-3</sup>.

Project	CFDE I	Temperature (°C)	CFDE III	Temperature (°C)
Observations	2301	-5.5 ± 4.0	5040	-6.9 ± 5.2
Liquid phase (%)	40	-4.1 ± 2.8	40	-5.1 ± 3.9
Mixed phase (%)	26	-4.9 ± 3.9	46	-7.3 ± 4.8
Glaciated phase (%)	34	-7.5 ± 4.6	14	-11.1 ± 6.8

cannot be segregated from the TWC signal. Cases with LWC below the RID LWC threshold of 0.01 g m<sup>-3</sup> cannot be differentiated from the glaciated cases, particularly if the droplet concentration measured on the FSSP is less than 15 cm<sup>-3</sup>. This LWC is also within the ±0.02 g m<sup>-3</sup> scatter in the LWC probes at small LWC values. Regardless, an LWC of 0.01 g m<sup>-3</sup> within any of the glaciated cases is sufficiently small in comparison with the average IWC measurements that it can be neglected. This may, however, confound the use of the FSSP for estimating ice concentrations in glaciated conditions.

Table 3 shows the percentages of liquid-, mixed-, and glaciated-phase conditions for CFDE I and III, as well as the mean and standard deviation of temperature for each block of data. There were substantially more mixed- and less glaciated-phase conditions in CFDE III than in CFDE I. This may be related to the cloud drop sizes or to the temperature. The relative fractions of liquid-, mixed-, and glaciated-phase cases for several temperature intervals, based on the collective CFDE I and III dataset, are shown in Fig. 12. As expected, the fraction of glaciated cases is a minimum near 0°C and increases steadily with decreasing temperature, whereas the fraction of liquid-phase cases is a maximum near 0°C and decreases with decreasing temperature. The fraction of mixed-phase cases is relatively constant from 0° to -20°C. A colder mean temperature in CFDE III would support an argument for a greater frequency of glaciated conditions, which is contrary to what was observed. The mean and standard deviation for ice crystal concentrations (≥125 μm in diameter) were 5 ± 5 and 4 ± 5 L<sup>-1</sup> for CFDE I and CFDE III, respectively. Because there were no distinct differences in the ice-crystal concentrations between the two projects, the colder temperatures during CFDE III, probably did not cause a greater activation of ice nuclei. It is unlikely that temperature effects account for the differences in the frequencies of mixed and glaciated phases between the two projects.

CFDE I was conducted in a maritime environment, whereas CFDE III was conducted in a continental environment. In CFDE I, the median droplet concentration for liquid-phase cases was 65 cm<sup>-3</sup>, with a median of the MVD of 24 μm. CFDE III had a median droplet concentration of 157 cm<sup>-3</sup> and a median of the MVD of 19 μm. Based only on the liquid-phase cases in which

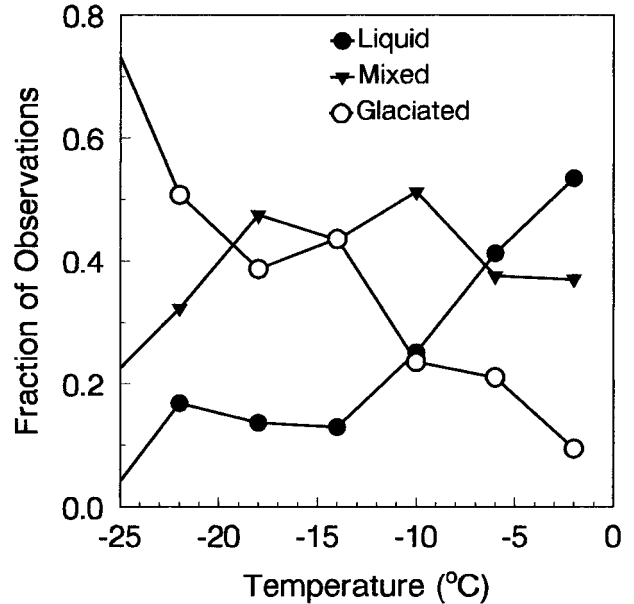


FIG. 12. Fraction of observations for each cloud phase as a function of temperature. The data were segregated into temperature intervals of 4°C.

contamination from ice crystals was negligible, 81% of the CFDE-I data were found to have droplets greater than 40 μm in diameter, as compared with 51% for the CFDE-III data. The observations are consistent with differences between maritime and continental clouds. The simultaneous presence of rimed ice particles and drops greater than 25 μm is a necessary condition for ice multiplication as discussed by Hallett and Mossop (1974). The Hallett and Mossop effect is primarily active between -4° and -8°C, accounting for 35%–40% of the in-cloud observations for CFDE I and III. These observations are generally consistent with the differences in Table 3. The concentrations of ice crystals greater than or equal to 125 μm in the temperature range from -4° to -8°C, in mixed and glaciated clouds, were not significantly different than for other temperature ranges, suggesting that other explanations are required. The different frequencies of mixed and glaciated observations may be partly the result of different cloud forcing mechanisms for the storms observed during the two projects.

Figure 13 shows the fraction of liquid water for the mixed-phase cases listed in Table 3. The calculations of IWC and LWC followed Eqs. (5) and (6). The error bar shows the average error associated with a liquid fraction calculation, although individual error estimates can be significantly higher. For cases that had significant mass in drops greater than 100 μm, the falloff of the LWC probes was estimated from Biter et al. (1987). The curves in Fig. 13 are relatively flat, increasing slightly toward higher liquid fraction values. There are no significant differences with temperature, except for the warmest temperature range at low liquid water fractions.

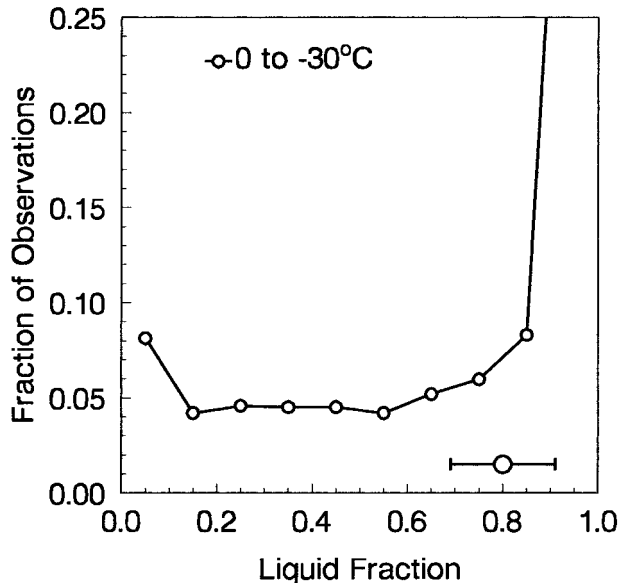


FIG. 13. Histograms of the liquid water fraction [ $LWC/(LWC + IWC)$ ] for 2925 mixed-phase cloud conditions observed during CFDE I and III. Each observation represents a 30-s average with the TWC  $\geq 0.01 \text{ g m}^{-3}$ , with a temperature between  $0^\circ$  and  $-30^\circ\text{C}$ . The error bar represents the mean error for a liquid fraction calculation.

Korolev and Isaac (2000) showed similar observations. At the warmer temperatures, the saturation vapor pressures between ice and water are closer together, which would allow droplets and ice to coexist for significantly longer periods of time. The data suggest that clouds can undergo a relatively constant rate of transition from liquid- to glaciated-phase conditions. This will be the subject of further research following Mazin et al. (2000). The mixed-phase clouds with liquid fractions greater than 0.9 primarily contain two distinct particle types: cloud drops with substantial LWC and ice crystals with very small IWC. These ice crystals tended to be relatively large ( $>500 \mu\text{m}$ ), which would be expected given that crystals in a water-saturated environment will generally grow rapidly. The cloud regions with liquid fractions less than 0.1 are mostly glaciated clouds with a small cloud droplet mode. If the definitions of a glaciated or liquid cloud, as defined in this discussion, were to be made more or less restrictive based on stronger or weaker instrument interpretations, the relative height of the peaks in liquid fraction in Fig. 13 for fractions greater than 0.9 and less than 0.1 would change. However, the trends in the data for  $0.1 < \text{liquid water fraction} < 0.9$  and the conclusions would not change.

## 6. Conclusions

In situ measurements in midlatitude winter clouds, from the First and Third Canadian Freezing Drizzle Experiments, were used to assess the relative responses to ice and liquid hydrometeors for several common instruments. These included the Rosemount icing detector,

PMS 2D-C mono and 2D-C gray probes, PMS FSSP on three separate measurement ranges, Nevzorov LWC and TWC probes, and PMS King LWC probe. The relative responses to ice and water are dependent on aircraft speed and ice-crystal size and concentration (Strapp et al. 1999), so the analysis may be restricted to the kinds of conditions observed during CFDE I and III.

Methods for assessing the relative ice and liquid responses for each instrument were developed, and the results were used to determine the relative frequency of liquid, mixed, and glaciated cloud conditions for each field project. Although the assessments of liquid, mixed, and glaciated are somewhat instrument dependent, lowering uncertainties in the assessments will not significantly change the conclusions.

Geometric formulas for particle diameter ratio, area ratio, perimeter ratio, perimeter-to-area ratio, and horizontal and vertical symmetry for images collected with PMS 2D probes were calibrated using drop images collected in clouds with temperatures greater than  $0^\circ\text{C}$ . These calibrations can be used to differentiate circular and noncircular images with reasonable accuracy. In liquid clouds these formulas identify more than 85% of the drops correctly for all sizes greater than or equal to 5 pixels in diameter. In glaciated clouds the formulas identify between 5% and 40% of the images as circular, depending on the pixel size. These circular ice particles are indistinguishable from water drops in mixed-phase or glaciated conditions, indicating that clear segregation of the ice and liquid particle spectra is still problematic. Improved accuracy could be obtained by increasing the size of the calibration dataset and performing separate calibrations for center-in and edge-element 2D processing techniques. A similar calibration technique could be applied to other particle shapes.

The Nevzorov and King LWC probes responded to between 5% and 30% of the IWC for the conditions observed. The average IWC response was 15% and 19% for the King and Nevzorov LWC probes, respectively. This result needs to be accounted for when computing IWC based on the TWC and LWC measurements.

In mixed-phase environments, the average FSSP spectrum was dominated by ice particles for sizes greater than  $35 \mu\text{m}$ , independent of the measurement ranges used. In a similar way, cloud droplets dominated the average measurements for sizes less than  $30 \mu\text{m}$ . Based on CFDE I and III observations, the measured droplet spectra should be truncated at  $35 \mu\text{m}$  for clouds in which the concentrations of ice particles were greater than  $1 \text{ L}^{-1}$ . In glaciated cloud conditions, concentrations of ice particles measured using an FSSP were found to be between 10 and 500 times the concentrations of particles greater than or equal to  $125 \mu\text{m}$  measured by the 2D probes. These observations are consistent with those of Gardiner and Hallett (1985) but could not be discounted as real measurements of small ice particles.

Methodologies for segregating liquid, mixed, and glaciated cloud regions were developed and applied to the

CFDE dataset. For cloud conditions with temperatures less than  $-4^{\circ}\text{C}$ , the method uses Nevzorov LWC and TWC, 2D-C, Rosemount icing detector, and FSSP instruments. The criteria can also be applied in the absence of an RID measurement and at warmer temperatures, although with reduced accuracy. Visual confirmation of the 2D analysis is useful in identifying cases in which the applied shape recognition algorithms might be misleading. When applied to the CFDE I and III datasets, identification of glaciated cloud regions was assessed when the instruments collectively demonstrated the following characteristics: ratio of LWC:TWC less than 0.25, fraction of circular 2D images greater than or equal to 125  $\mu\text{m}$  less than 0.35, FSSP MVD greater than 30  $\mu\text{m}$ , and FSSP concentrations less than  $15\text{ cm}^{-3}$ . Liquid-phase conditions were assessed for LWC:TWC ratio greater than 0.85, fraction of circular 2D images greater than 0.85, and concentration of noncircular 2D images less than  $0.1\text{ L}^{-1}$ . At temperatures less than  $-4^{\circ}\text{C}$ , a Rosemount icing-detector threshold of  $2\text{ mV s}^{-1}$  was also used to differentiate glaciated and nonglaciated cloud conditions. For both the CFDE I and III datasets, approximately 40% of the in-cloud observations at temperatures less than  $0^{\circ}\text{C}$  were assessed as liquid phase. The fractions of mixed-phase and glaciated-phase conditions were 26% and 34% for CFDE I, and 46% and 14% for CFDE III, respectively.

The CFDE I and III data were collected primarily to assess the aircraft icing environments associated with supercooled large drops greater than 50  $\mu\text{m}$  in diameter. In mixed-phase conditions for which the concentration of ice crystals were greater than  $1\text{ L}^{-1}$ , there are two problems: 1) the average FSSP spectra were dominated by liquid droplets only to about 35  $\mu\text{m}$ , above which they could be significantly biased by ice crystals, and 2) the identification of circles (i.e., drops) with the 2D instruments has large uncertainties for sizes up to at least 10 pixels (250  $\mu\text{m}$ ). The implication is that the measured droplet spectra for these cases must be interpolated between 35 and 275  $\mu\text{m}$ , which may introduce considerable errors and which incorporates a large portion of any drizzle spectrum. This limitation applies to approximately 30% (1000 of the 30-s observations) of the mixed-phase conditions observed during CFDE I and III. The results of other aircraft icing characterizations (Miller et al. 1998; Ashenden and Marwitz 1998; Bain and Gayet 1982; Sand et al. 1984) may be affected in a similar manner.

*Acknowledgments.* This work was supported by the Canadian National Search and Rescue Secretariat, Transport Canada, the National Research Council (NRC), the Meteorological Service of Canada (MSC), and Boeing Commercial Airplane Group. The authors acknowledge the technicians of MSC and NRC for their hard work in keeping the data systems and instrumentation working and calibrated. Dave Marcotte of NRC

is acknowledged for his contributions during the project planning and measurement phases.

#### REFERENCES

- Ashenden, R., and J. D. Marwitz, 1998: Characterizing the supercooled large droplet environment with corresponding turboprop aircraft response. *J. Aircraft*, **35**, 912–920.
- Bain, M., and J. F. Gayet, 1982: Aircraft measurements of icing in supercooled and water droplet/ice crystal clouds. *J. Appl. Meteor.*, **21**, 631–641.
- Baumgardner, D., 1983: An analysis and comparison of five water droplet measuring instruments. *J. Climate Appl. Meteor.*, **22**, 891–910.
- , and A. Rodi, 1989: Laboratory and wind tunnel evaluations of the Rosemount icing detector. *J. Atmos. Oceanic Technol.*, **6**, 971–979.
- , W. Strapp, and J. E. Dye, 1985: Evaluation of the forward scattering spectrometer probe. Part II: Corrections for coincidence and dead time losses. *J. Atmos. Oceanic Technol.*, **2**, 626–632.
- Biter, C. J., J. E. Dye, D. Huffman, and W. D. King, 1987: The drop-size response of the CSIRO liquid water probe. *J. Atmos. Oceanic Technol.*, **4**, 359–367.
- Cober, S. G., G. A. Isaac, and J. W. Strapp, 1995: Aircraft icing measurements in East Coast winter storms. *J. Appl. Meteor.*, **34**, 88–100.
- , J. W. Strapp, and G. A. Isaac, 1996: An example of supercooled drizzle drops formed through a collision-coalescence process. *J. Appl. Meteor.*, **35**, 2250–2260.
- , G. A. Isaac, and A. V. Korolev, 2001: Assessing the Rosemount icing detector with in situ measurements. *J. Atmos. Oceanic Technol.*, **18**, 515–528.
- Drummond, A. M., and J. I. MacPherson, 1985: Aircraft flow effects on cloud drop images and concentration measured by the NAE Twin Otter. *J. Atmos. Oceanic Technol.*, **2**, 633–643.
- Fowler, L. D., and D. A. Randall, 1996: Liquid and ice cloud microphysics in the CSU general circulation model. Part III: Sensitivity of modeling assumptions. *J. Climate*, **9**, 561–586.
- Gardiner, B. A., and J. Hallett, 1985: Degradation of in-cloud forward scattering spectrometer probe measurements in the presence of ice particles. *J. Atmos. Oceanic Technol.*, **2**, 171–180.
- Hallett, J., and S. C. Mossop, 1974: Production of secondary ice particles during the riming process. *Nature*, **249**, 26–28.
- Heymsfield, A. J., and J. L. Parrish, 1978: A computational technique for increasing the effective sampling volume of the PMS two-dimensional particle size spectrometer. *J. Appl. Meteor.*, **17**, 1566–1572.
- , and L. M. Miloshevich, 1989: Evaluation of liquid water measuring instruments in cold clouds sampled during FIRE. *J. Atmos. Oceanic Technol.*, **6**, 378–388.
- Isaac, G. A., S. G. Cober, A. V. Korolev, J. W. Strapp, A. Tremblay, and D. L. Marcotte, 1998: Overview of the Canadian Freezing Drizzle Experiment I, II, and III. Preprints, *Conf. on Cloud Physics*, Everett, WA, Amer. Meteor. Soc., 447–450.
- Joe, P., and R. List, 1987: Testing and performance of two-dimensional optical array spectrometers with greyscale. *J. Atmos. Oceanic Technol.*, **4**, 139–150.
- King, W. D., 1986: Air flow around PMS canisters. *J. Atmos. Oceanic Technol.*, **3**, 197–198.
- , D. A. Parkin, and R. J. Handsworth, 1978: A hot wire liquid water device having fully calculable response characteristics. *J. Appl. Meteor.*, **17**, 1809–1813.
- , J. E. Dye, J. W. Strapp, D. Baumgardner, and D. Huffman, 1985: Icing wind tunnel tests on the CSIRO liquid water probe. *J. Atmos. Oceanic Technol.*, **2**, 340–352.
- Korolev, A. V., and G. A. Isaac, 2000: Phase composition of stratiform clouds. *Proc. 13th Int. Conf. on Clouds and Precipitation*, Reno, NV, 725–727.

- , and B. Sussman, 2000: A technique for habit classification of cloud particles. *J. Atmos. Oceanic Technol.*, **17**, 1048–1057.
- , J. W. Strapp, and G. A. Isaac, 1998a: Evaluation of the accuracy of PMS optical array probes. *J. Atmos. Oceanic Technol.*, **15**, 708–720.
- , —, —, and A. N. Nevzorov, 1998b: The Nevzorov airborne hotwire LWC–TWC probe: Principles of operation and performance characteristics. *J. Atmos. Oceanic Technol.*, **15**, 1495–1510.
- Ludlam, F. H., 1951: The heat economy of a rimed cylinder. *Quart. J. Roy. Meteor. Soc.*, **77**, 663–666.
- Mazin, I. P., A. V. Korolev, and G. A. Isaac, 2000: Phase transformation in clouds. *Proc. 13th Int. Conf. on Clouds and Precipitation*, Reno, NV, 657–660.
- , —, A. Heymsfield, G. A. Isaac, and S. G. Cober, 2001: Thermodynamics of icing cylinder for measurements of liquid water content in supercooled clouds. *J. Atmos. Oceanic Technol.*, **18**, 543–558.
- Miller, D., T. Ratvasky, B. Bernstein, F. McDonough, and J. W. Strapp, 1998: NASA/FAA/NCAR supercooled large droplet icing flight research: Summary of winter 96–97 flight operations. *AIAA 36th Aerospace Science Meeting and Exhibit*, Reno, NV, AIAA Paper 98-0577.
- Rauber, R. M., and M. F. Heggli, 1988: The influence of cloud droplets on the measurement of ice particle concentrations with a Particle Measuring System's 2DC optical array probe. *J. Atmos. Oceanic Technol.*, **5**, 123–128.
- Riley, R. K., 1998: Mixed-phase icing conditions: A review. U.S. Dept. of Transportation Rep. DOT/FAA/AR-98/76, 45 pp.
- Rotstayn, L. D., 1997: A physically based scheme for the treatment of stratiform clouds and precipitation in large-scale models. Part 1: Description. *Quart. J. Roy. Meteor. Soc.*, **123**, 1227–1282.
- Sand, W. R., W. A. Cooper, M. K. Politovich, and D. L. Veal, 1984: Icing conditions encountered by a research aircraft. *J. Climate Appl. Meteor.*, **23**, 1427–1440.
- Strapp, J. W., P. Chow, M. Maltby, A. D. Bezer, A. V. Korolev, I. Stromberg, and J. Hallett, 1999: Cloud microphysical measurements in thunderstorm outflow regions during Allied/BAE 1997 flight trials. *AIAA 37th Aerospace Science Meeting and Exhibit*, Reno, NV, AIAA Paper 99-0498.
- , J. Oldenburg, R. Ide, Z. Vukovic, S. Bacic, and L. Lilie, 2000: Measurements of the response of hot wire LWC and TWC probes to large droplet clouds. *Proc. 13th Int. Conf. on Clouds and Precipitation*, Reno, NV, 181–184.
- , F. Albers, A. Reuter, A. V. Korolev, W. Maixner, E. Rashke, and Z. Vukovic, 2001: Laboratory measurements of the response of a PMS OAP-2DC probe. *J. Atmos. Oceanic Technol.*, **18**, 1150–1170.
- Sun, Z., and K. P. Shine, 1994: Studies of the radiative properties of ice and mixed-phase clouds. *Quart. J. Roy. Meteor. Soc.*, **120**, 111–137.
- Tremblay, A., A. Glazer, Y. Wei, and R. Benoit, 1996: A mixed-phase cloud scheme based on a single prognostic equation. *Tellus*, **48A**, 483–500.
- Young, S. A., C. M. R. Platt, R. T. Austin, and G. R. Patterson, 2000: Optical properties and phase of some midlatitude, midlevel clouds in ECLIPS. *J. Appl. Meteor.*, **39**, 135–153.